This is the Authors' Accepted Manuscript version of the paper:
E. Hyeon, Y. Kim, T. Ersal, and A. Stefanopoulou, "Data-driven forgetting and discount factors for vehicle speed forecasting in ecological adaptive cruise control," Journal of Dynamic Systems Measurement and Control, vol. 144, no. 1, pp. 011101 (12 pages), 2022.
doi: 10.1115/1.4052272

Data-Driven Forgetting and Discount Factors for Vehicle Speed Forecasting in Ecological Adaptive Cruise Control

Eunjeong Hyeon
Department of Mechanical Engineering
University of Michigan
Ann Arbor, Michigan 48109
ejhyeon@umich.edu

Youngki Kim
Department of Mechanical Engineering
University of Michigan-Dearborn
Dearborn, Michigan 48128
youngki@umich.edu

Tulga Ersal
Department of Mechanical Engineering
University of Michigan
Ann Arbor, Michigan 48109
tersal@umich.edu

Anna Stefanopoulou
Department of Mechanical Engineering
University of Michigan
Ann Arbor, Michigan 48109
annastef@umich.edu

This paper investigates temporal correlations in human driving behavior using real-world driving to improve speed forecasting accuracy. These correlations can point to a measurement weighting function with two parameters: a forgetting factor for past speed measurements that the vehicle itself drove with, and a discount factor for the speeds of vehicles ahead based on information from vehicle-to-vehicle (V2V) communication. The developed weighting approach is applied to a vehicle speed predictor using polynomial regression, a prediction method well-known in the literature. The performance of the developed approach is then assessed in both real-world and simulated traffic scenarios for accuracy and robustness. The new weighting method is applied to an ecological adaptive cruise control system, and its influence is analyzed on the prediction accuracy and the performance of the eco-ACC in an electric vehicle powertrain model. The results show that the new prediction method improves energy saving from the eco-driving by up to 4.7% compared to a baseline least-square-based polynomial regression. This is a 10% improvement over the constant speed/acceleration model, a conventional speed predictor.

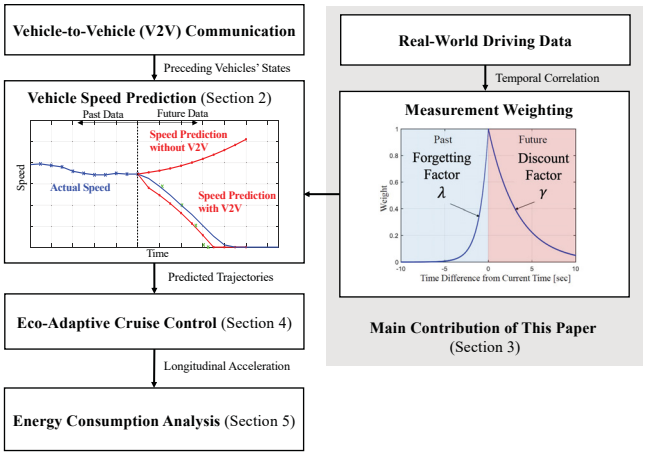

Fig. 1. Overview of this paper.

1 Introduction

In typical traffic environments, one vehicle's energy efficiency can be highly influenced by the driving patterns of the immediate preceding vehicle. Thus, many studies have proposed designs of ecological adaptive cruise control (eco-ACC) systems based on predictive control techniques that optimize the controlled vehicle's longitudinal maneuvers by predicting the future behavior of its immediate preceding vehicle [1–3]. These predictive eco-ACC strategies solve constrained optimal control problems over the horizon with previews anticipating the future driving environment, such as the immediate preceding vehicle's trajectory. As inaccurate previews could degrade the controlled vehicle's fuel economy down to levels even worse than human driving [4–6], obtaining accurate previews of the preceding vehicle's future states is essential to maximize the performance of eco-ACC.

With the recent improvements in on-road sensors and communication technologies, data-driven forecasting approaches have been widely studied for predicting a human-driven vehicle's future trajectories. Conventional time-series forecasting methods that have been used to predict a vehicle's velocity include an auto-regressive integrated moving average model [7, 8], an auto-regressive model with external input [8, 9], artificial neural networks [10–14], and a long

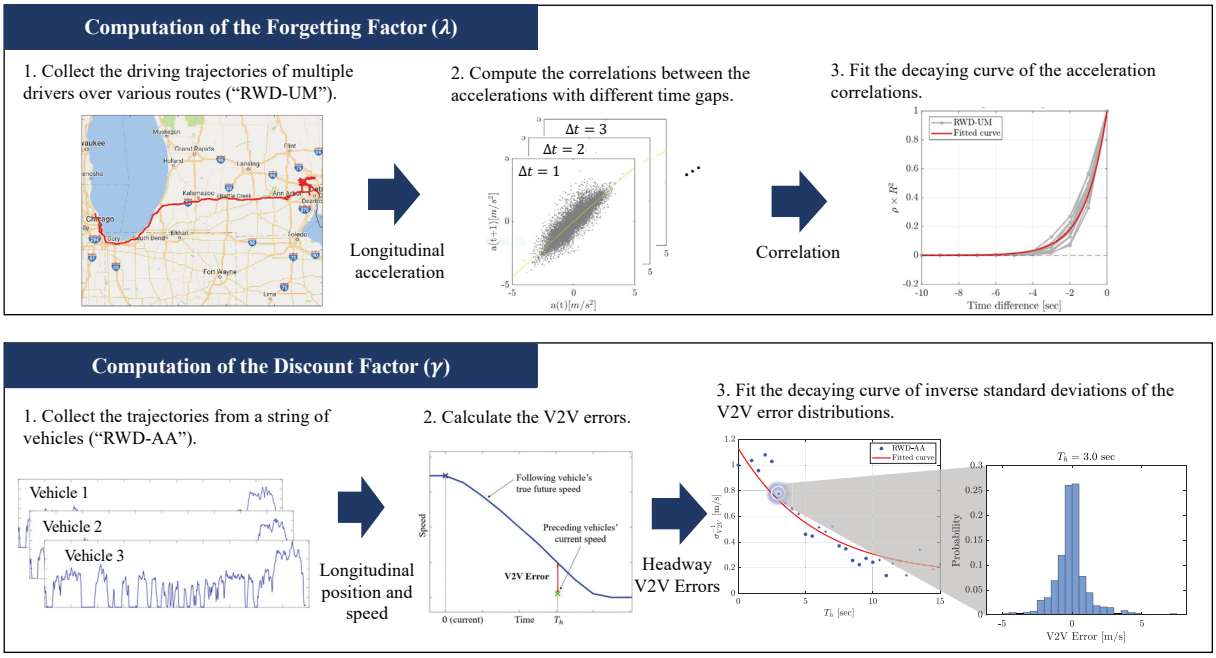

Fig. 2. Flowcharts of the processes to obtain the weighting parameters, the forgetting factor (top) and the discount factor (bottom), respectively. Detailed explanation of these processes are presented in Section 3.2 and 3.3.

short-term memory network [8, 15]. Stochastic prediction approaches have been developed, such as a Markov chain model based on the past acceleration of the predicted vehicle [8,16,17]. A conditional linear Gaussian model has also been studied based on measurements obtained by a radar and V2V and vehicle-to-infrastructure (V2I) communications [8, 18]. In addition, more complex predictors have been explored that combine regression and probabilistic approaches to enhance prediction accuracy [19–21].

In general, the learning-based forecasting techniques are powerful but only when an enormous amount of training data is available. When no historical information is available, earlier efforts have developed rule-based methods that do not require a learning process. The simplest rule-based methods are constant speed and acceleration models that propagate a predicted vehicle's current speed or acceleration over a prediction horizon [11]. In more elaborate versions, some previous work has modeled human drivers' actions based on their characteristics. For example, the authors in [22] have modeled human driver's pedaling motion based on their observations that most drivers applied acceleration with exponentially decaying patterns. Other researchers selected a sigmoid function to model human driver's acceleration demands [23]. Microscopic traffic models such as an intelligent driver model [24] also have been utilized to generate the estimated trajectory of a preceding vehicle based on the current states [11, 25–27]. In [10], polynomial regression is used to predict speed trajectories of 2 seconds (s) by estimating polynomial coefficients based on the past measurements only. In [28], the enhanced version of the polynomial regression method is developed by using V2V information, which allows the predictor to compute 10 s speed profiles with high accuracy. Researchers also have used locally-weighted polynomial regression of V2V and V2I messages and calculated more extended predictions (50 s) [29].

While the complex data-driven methods can learn measurement weights through their algorithms, no schemes are given for weighting measurements in the aforementioned rule-based methods and simple regression techniques. To our best knowledge, there are no studies that have addressed the methodologies of weighting measurements for predicting vehicle future speed.

Recognizing that gap, this work proposes a novel measurement weighting method to prioritize information sampled from different times and sources. The overview of the paper is illustrated in Fig. 1. First, an exponentially-decaying function is developed as a measurement weighting function based on temporal correlations in real-world driving records. The decaying rates are defined as a "forgetting factor" for the past information and a "discount factor" for the future information. Those parameters are determined from two sets of real-world speed data: 1) to guide the forgetting factor, a set of driving data collected by the University of Michigan Transportation Research Institute as a part of the Integrated Vehicle-Based Safety Systems (RWD-UM) is used, and 2) to determine the discount factor, a set of data including three human-driven vehicles' trajectories, closely following each other on the same lane during an entire trip in Ann Arbor (RWD-AA) is analyzed. The methodologies for these data analyses are illustrated in Fig. 2.

To assess the benefits of the developed weighting method, a simple eco-ACC problem based on model predictive control (MPC) is implemented and tested in simulations, where various driving scenarios are considered. The predictor produces the immediate preceding vehicle's speed trajectory, and the speed is integrated to obtain position, which is then fed into the eco-ACC problem. Two types of test data are used to evaluate the performance of the new method compared to other rule-based or conventional approaches. Energy consumption is calculated for an electric vehicle powertrain by using the vehicle simulator Autonomie [30]. The results show that by applying the new weighting method, electricity consumption can be reduced by up to 4% compared to the regular least-squares estimation. The main contributions of this paper are therefore as follows:

1. A measurement weighting strategy is developed for vehicle speed predictors that do not have dedicated optimization rules for the weights on measurements or input features.
2. To design a measurement weighting function, systematic data analyses are conducted to find temporal correlations in the human driving states from historical driving data.
3. The predictor developed in [28] is implemented with the new weighting method. Then, the predictor is simulated with an eco-ACC and compared with baseline predictors in terms of energy consumption and tracking capability.
4. The robustness of the predictor is demonstrated by testing it in a real-world traffic scenario and a simulated driving environment with various traffic conditions.

The rest of this paper is organized as follows. Section 2 explains the prediction algorithm based on polynomial regression. Section 3 describes the novel measurement weighting method based on human driving data. In Section 4, the eco-ACC problem implemented for this work is described. Simulation settings and results are presented in Section 5. Finally, Section 6 summarizes the contributions of this paper and introduces future work.

2 Vehicle Speed Forecasting Method

In our application of interest, a prediction target is the future speed of the immediate front vehicle (target vehicle) of the controlled vehicle (ego vehicle). The speed predictor used in this paper is developed in our previous paper [28]. The key idea of our prediction method is to infer the near-future speed trajectory of the target vehicle based on the driving history of the target and the current traffic speed in front. Two types of information are utilized to predict the target vehicle's future speed:

1. Past speed trajectories of the target vehicle.
2. Current speed and location of the target and the preceding vehicles.

The first type of data can be obtained through the ego vehicle's sensor, such as radar. The second type of data is assumed to be available through V2V communication. Here, the preceding vehicles are the vehicles driving in front of the target vehicle on the same lane.

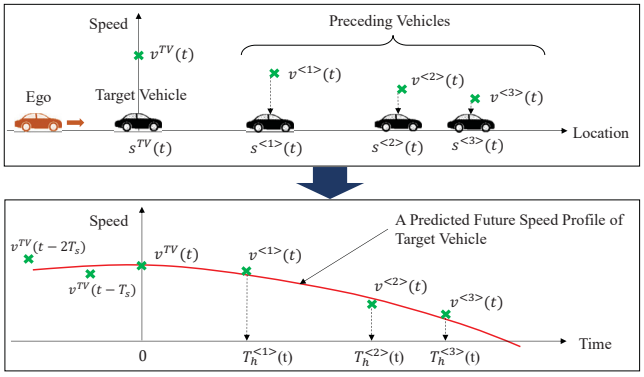

Fig. 3. Pictorial description of the developed speed forecasting method and its fitting domain. The solid line in the bottom box represents the future speed profile of the target vehicle fitted with measurements (the cross markers).

In Fig. 3, the definition of the ego, target, and preceding vehicles, and the prediction process with the prediction domain are depicted. The position information of the preceding vehicles is converted to the estimated time of arrival (ETA) of the ego vehicle at their location. In this work, ETA is computed as the time headway to a preceding vehicle:

$$T_h^{<j>}(t) = \frac{s^{<j>}(t) - s^{TV}(t)}{\max(v^{TV}(t),\, \underline{v})}, \tag{1}$$

where $s^{<j>}(t)$ and $s^{TV}(t)$ are the current location of the j^{th} preceding vehicles and the target vehicle, respectively. In the denominator, $v^{TV}(t)$ represents the current speed of the target vehicle. $\underline{v}$ is imposed to bound the ETA value in a reasonable range when v^{TV} is near zero, and here, $\underline{v} = 5$ m/s. The processed information is used as one of the input in the prediction algorithm.

Quadratic polynomial regression generates the predicted speed profile over a short horizon. A speed prediction at the k^{th} step in a prediction horizon is calculated as:

$$\hat{v}^{TV}(k|t) = \beta_0(t) + \beta_1(t)\cdot kT_s + \beta_2(t)\cdot (kT_s)^2. \tag{2}$$

In (2), $k|t$ represents that the variable is the k^{th}-step prediction when the current time is t; i.e., the variable is the future estimate at $t + k\cdot T_s$, where T_s is the sampling time. Here, if the number of collected measurements is fewer than three, a linear polynomial fit is used for regression quality. The coefficients of the quadratic polynomial $\beta(t) = [\beta_0(t),\, \beta_1(t),\, \beta_2(t)]^T$ are determined using the weighted least-squares (WLS) estimation method:

$$\beta(t) = \arg\min \left\| W^{1/2}\left(\hat{\mathbf{v}} - \mathbf{v}(t)\right)\right\|_2^2 \tag{3}$$

Fig. 4. An example of routes traveled by one of the human drivers in the RWD-UM dataset.

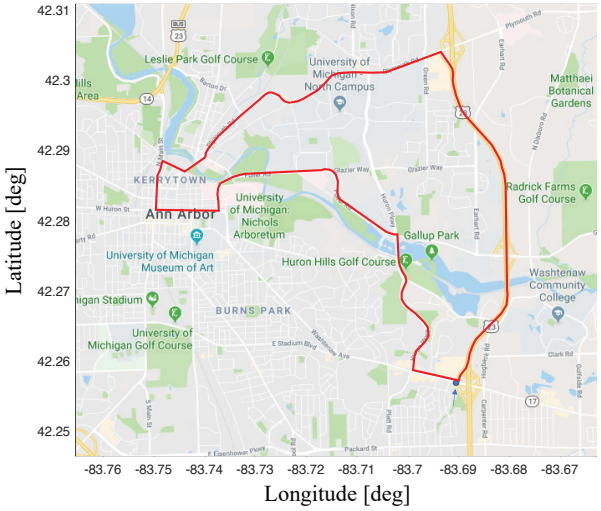

Fig. 5. The route driven by the three vehicles in the RWD-AA dataset. The map shows the Ann Arbor area in Michigan.

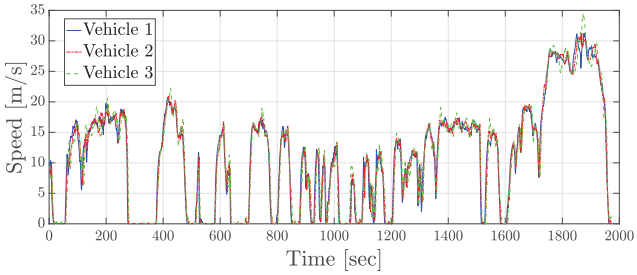

Fig. 6. Speed profiles of the three vehicles in the RWD-AA data.

where $\mathbf{v}(t)$ is a measurement vector and a measurement weight matrix W. In this work, measurement weights are determined from data observations. Specifically, a weight on the i^{th} measurement, w_i, is determined by the following equations:

$$w_i = \begin{cases} \lambda^{(N_{past}-i+1)T_s} & \text{if the } i^{th} \text{ measurement is the past speed of the target vehicle,} \\ \gamma^{T_h^{<j>}} & \text{otherwise.} \end{cases} \quad (4)$$

Here, λ is defined as the forgetting factor of the target vehicle's past speed, γ is the discount factor of the preceding vehicles' current speed, and both parameters satisfy: $0 < \lambda \leq 1$ and $0 < \gamma \leq 1$. Hence, both weighting functions exponentially decay over time. This shape is designed based on our hypothesis about data: as the gaps of time or distance from the data sources become larger, the correlations between future speed and the fitting data would decay exponentially. The decaying rates are determined by two parameters: the forgetting and the discount factors. The designs of the forgetting and discount factors are the key contributions of this paper and each design process is introduced in the following section.

3 Data-Driven Measurement Weights using Real-World Driving Records

In this section, the design methodology for the measurement weight matrix, W, in (3) is described. The main idea is to analyze the temporal correlations between measurements and prediction targets and model a measurement weighting function based on our data analysis. In the following section, the real-world driving records used for this analysis are described.

3.1 Real-World Driving Data

To design the measurement weight matrix, W, real-world driving datasets were analyzed. This work used two types of datasets whose detailed information is given as follows:

RWD-UM: The RWD-UM dataset was collected and provided by the University of Michigan Transportation Research Institute (UMTRI) as a part of the Integrated Vehicle-Based Safety Systems (IVBSS) program [31]. In these datasets, human-driven vehicles' driving states in various conditions including city and highway driving were recorded by their on-board sensors. The vehicle models used in the experiments were 2006 and 2007 Honda Accord EX four-door sedans. Preceding vehicles' driving states are not available in these datasets. The example trajectories driven by a driver are plotted on the map in Fig. 4. In this work, longitudinal speed and acceleration information from 1668 trips driven by ten human drivers are utilized. These datasets are used for determining weights on the past measurements of the predicted vehicle in Section 3.2.

RWD-AA: The RWD-AA data was collected by Toyota Motor North America in Ann Arbor, Michigan. The data include three human-driven vehicles' trajectories, closely following each other on the same lane during an entire trip. The route is plotted in Fig. 5, and the speed profile of each vehicle is presented in Fig. 6. The route includes both city and highway sections, and the total trip time was about 30 minutes. The vehicles used in the experiment were four-door sedans.

The vehicles were equipped with dedicated short-range communication (DSRC) transmitters and receivers. In the experiments, the vehicles were capable of communicating with each other. The speed and position trajectories transmitted in DSRC basic safety messages by the three vehicles are used for this work. This dataset is used for tuning weights on the V2V measurements. Details on this process are reported in Section 3.3. In addition, the data are utilized to reproduce the realistic traffic for our simulation introduced in Section 5. This platooning dataset is chosen for our analysis, because it has the sufficient length of trip for comparing energy consumption by human driving and eco-ACC.

It is noted that both RWD-UM and RWD-AA datasets were collected from the similar vehicle classes, which are four-door sedans. Thus, the influence of a vehicle class on driving styles is assumed to be negligible in our data analyses.

3.2 Information from Past Speed Measurements

For the past measurements, the temporal correlation of longitudinal acceleration is analyzed, because the predictor based on the polynomial regression estimates future speed based on the trend in the past speed measurements. The RWD-UM datasets are used to analyze the correlations of acceleration. To consider various driving styles, we used driving records collected from ten different human drivers. Each vehicle drove different routes, mainly in the North East and a few in the South East areas in the United States. The correlation is computed for high-speed and low-speed driving separately. To divide the high-speed and low-speed sections in trips, the speed criterion of 60 mile-per-hour (mph) is adopted from [32], which is one of the typical speed limits on highways in the United States.

The accelerations with different time gaps are presented by the scatter plots in Fig. 7 and 8 for the low-speed and high-speed sections, respectively. In these results, the relationships between accelerations with different time gaps from 1 to 5 s are shown. Both figures show that the correlation between accelerations rapidly decreases as the time gap increases. The correlation coefficients (ρ) multiplied by the coefficients of determination (R^2) are plotted in Fig. 9. The left subplot shows the product of the correlation coefficient and the coefficient of determination ($\rho \cdot R^2$) from the low-speed sections, and the right subplot presents the results from the high-speed parts. The lines with the dot markers are actual statistics from the ten drivers' trips in the RWD-UM data, and the solid lines fit the statistics.

3.3 Look-ahead Information from V2V Measurements

In a typical traffic environment, as the locations of two vehicles become closer, their speed trajectories become more similar. Thus, for the speed measurements transmitted from the preceding vehicles, the correlations between two vehicles' speeds are studied. Since our predictor maps the preceding vehicles' speed onto the fitting domain based on ETA, we define "V2V errors," which is a new concept introduced to define the temporal correlation between two vehicle's speed profiles with respect to ETA. The V2V error is defined as follows:

Table 1. Summary of Prediction Parameter Tuning

Type	Low speed (<60 mph)	High speed (≥ 60 mph)
Forgetting factor (λ)	0.51	0.43
Discount factor (γ)	0.77	0.71

$$\text{V2V Error} = v^{FV}(t+T_h) - v^{LV}(t) \tag{5}$$

where $v^{FV}(t+T_h)$ is the speed of a following vehicle at time $t+T_h$ and v^{LV} is the speed of a lead vehicle at time t. T_h is the time headway from the lead vehicle to the following vehicle, which is used as ETA in our prediction process. The intuitive meaning of the V2V errors is the mismatch between the lead car's current speed and the following car's future speed when the following car arrives at the lead's location, since time headway is used as the estimated time of arrival to the preceding car's location in our predictor.

The V2V errors are produced from the RWD-AA data. The statistics of V2V errors are presented in Fig. 10. The standard deviation of the V2V errors are calculated with the measurement samples within the time headway window of 0.5 s. In Fig. 10, the blue asterisks show the inverse standard deviations of the V2V errors for every time headway window. The red curves fit the trend of the inverse standard deviations of V2V errors with different time headway.

The observation of the data in Figs. 9 and 10 points to an exponentially decaying function versus time as defined in (4). Hence, the forgetting and discount factors represent the decaying rates of the curves in Fig. 9 and 10, and their values are summarized in Tab. 1.

4 Ecological Adaptive Cruise Control

Since eco-ACC, typically formulated in a model predictive control scheme, relies on the future speed information, it is considered as a good example application to evaluate the performance of the proposed weighting method in speed forecasting. Thus, this section describes the formulation of an optimal control problem for the eco-ACC used in this work. The definitions of the ego, target, and preceding vehicles are the same with the ones illustrated in Fig. 3.

4.1 Vehicle Dynamics

Since the main focus of this paper is energy savings in car-following scenarios, only the longitudinal dynamics of the ego vehicle are considered. For simplicity, we assume that no lane changes occur. Furthermore, the dynamics are simplified with the assumption of negligible road grades as

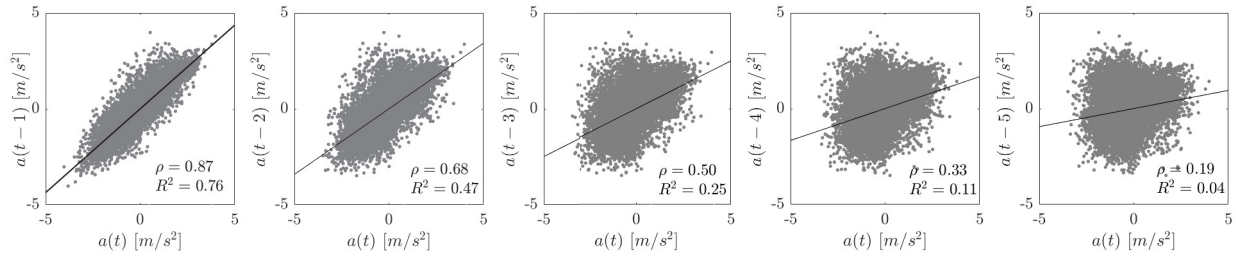

Fig. 7. Accelerations with different time gaps at low-speed sections in the real-world driving records traveled by the UMTRI driver 1.

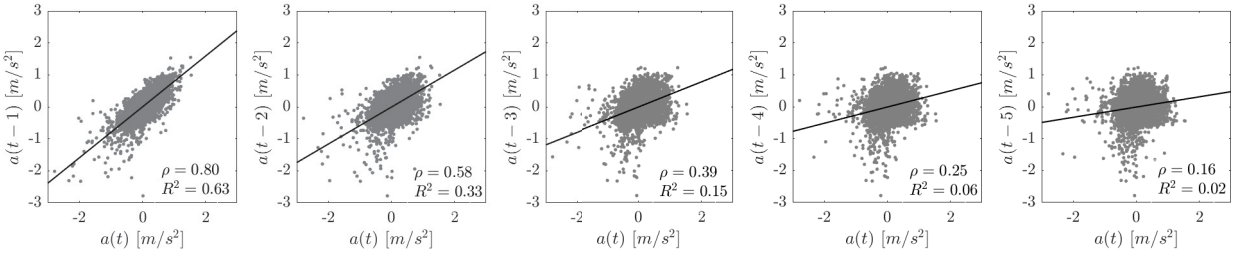

Fig. 8. Accelerations with different time gaps at high-speed sections in the real-world driving records traveled by the UMTRI driver 1.

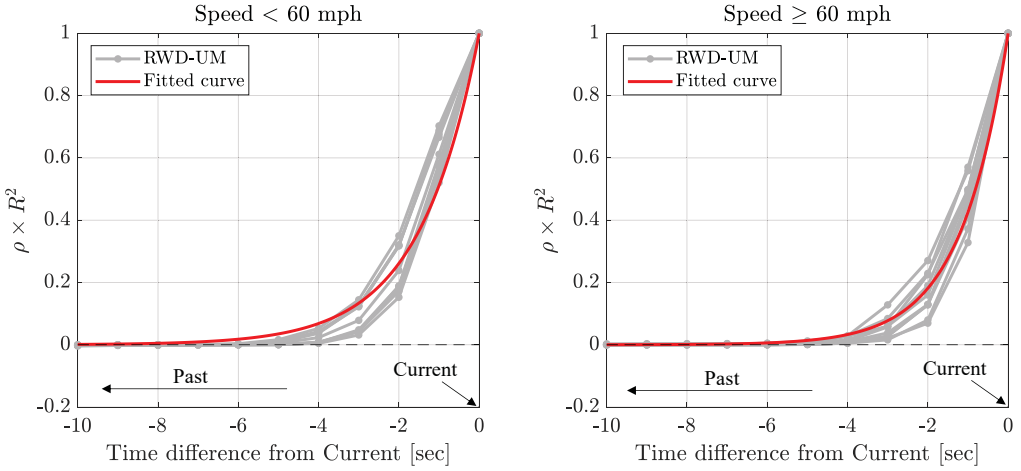

Fig. 9. Calculations between correlation and coefficient of determination of linear fit between accelerations with time differences. Ten human drivers' driving records from the RWD-UM datasets are included in this analysis. The solid lines are the fitted curves of results from real data that are plotted in the lines with the dot markers.

follows:

$$\dot{s} = v \tag{6a}$$

$$\dot{v} = \frac{1}{m}\left(F_t - mgC_r - \frac{1}{2}\rho A_f C_d v^2 - F_b\right) \tag{6b}$$

where s and v are the longitudinal position and velocity of a vehicle, respectively. m denotes the vehicle mass, F_t indicates the traction force, and g is the gravitational acceleration. C_r and C_d represent the rolling resistance coefficient and the air drag coefficient, respectively. ρ denotes the air density, A_f indicates the vehicle frontal area, and F_b represents the braking force. The above model is discretized to obtain:

$$s(k+1) = s(k) + v(k)\cdot T_s + u_p(k)\cdot T_s^2 \tag{7a}$$

$$v(k+1) = v(k) + u_p(k)\cdot T_s \tag{7b}$$

$$u_p(k) = u(k) - gC_r - \frac{1}{2m}\rho A_f C_d v(k)^2 \tag{7c}$$

where u is an acceleration command, which is the solution of the optimal control problem described in the next section. The symbol u encompasses deceleration by allowing it to have a negative sign. We use the term "acceleration" to indicate both acceleration and deceleration for simplicity in the rest of the paper. The equations in (7) are used as a plant model in our simulations.

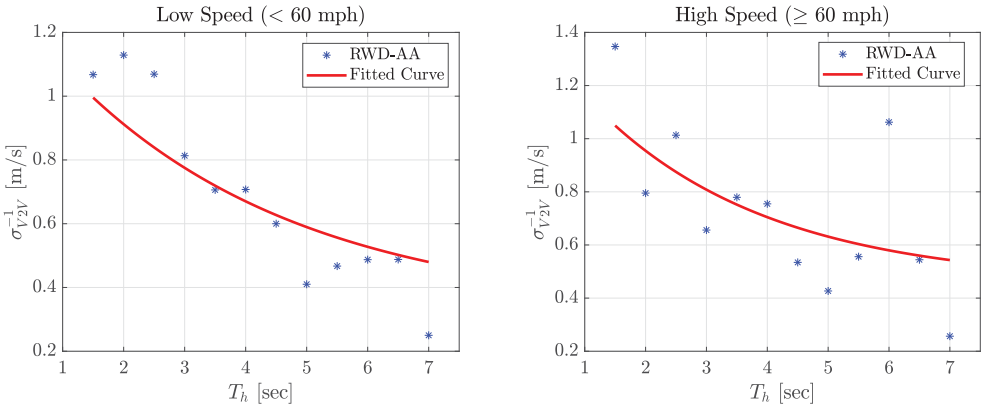

Fig. 10. Inverse standard deviations of the V2V errors with different time headway between preceding and following vehicles from the RWD-AA data. The data were used for designing the discount factor (γ).

4.2 Optimal Control Problem

The eco-ACC is realized by minimizing the control efforts, the surrogate optimization problem of energy minimization, by penalizing the square sum of longitudinal acceleration. This approach allows us to formulate the optimization problem as a quadratic programming. The optimal control problem is derived as follows:

$$\min_{u,\xi} \quad J \tag{8a}$$

$$\text{s.t.} \quad s(k|t) \le \hat{s}^{TV}(k|t) - v(k|t)T_h^* - L - d^* + \xi(t), \tag{8b}$$

$$v_{min} \le v(k|t) \le v_{\max}, \tag{8c}$$

$$u_{\min} \le u(k|t) \le u_{\max}, \tag{8d}$$

$$\xi(t) \ge 0, \tag{8e}$$

$$s(k+1|t) = s(k|t) + v(k|t)T_s + 0.5u(k|t)T_s^2 \tag{8f}$$

$$v(k+1|t) = v(k|t) + u(k|t)T_s \tag{8g}$$

where the objective function of the eco-ACC is formulated as follows:

$$\begin{aligned} J = &\sum_{k=1}^{N_p} \phi_s(\hat{s}^{TV}(k|t) - s(k|t) - v(k|t)T_h^* - L - d^*)^2 \\ &+ \sum_{k=1}^{N_p} \phi_v(t) \cdot (v(k|t) - v^*(k|t))^2 \\ &+ \sum_{k=0}^{N_p-1} \phi_u u(k|t)^2 + \phi_\xi \xi(t)^2. \end{aligned} \tag{9}$$

In (8) and (9), $k|t$ represents that the variable is the k^{th}-step prediction when the current time is t as in (2). T_s is the sampling time and N_p is the number of steps in a prediction horizon. The variables s and v are the ego vehicle's longitudinal position and velocity, respectively. $\hat{s}^{TV}$ is the target vehicle's longitudinal position estimate predicted by the ego vehicle. d^* is a marginally safe distance between the lead and ego vehicles for safety, T_h^* is the desired time headway, and v^* is the desired speed, which is set to the speed limit. $\xi(t)$ is a slack variable imposed to soften the positional constraints to achieve recursive feasibility.

Table 2. Parameters in MPC Formulation

Type	Unit	Notation	Value
Car Length	meters	L	4.5
Marginal distance gap	meters	d^*	2
Desired headway	second	T_h^*	2
Max. acceleration	m/s^2	$u_{\max}$	4
Min. acceleration	m/s^2	$u_{\min}$	-4
Max. speed	m/s	$v_{\max}$	40
Min. speed	m/s	$v_{\min}$	0

The objective function (9) is composed of four terms. The first term, multiplied by a penalty coefficient of ϕ_s, ensures a safe distance gap from the target vehicle by following the desired time headway. The second term with a coefficient of ϕ_v recommends following the speed limit imposed on the road section. The third term, multiplied by a penalty coefficient of ϕ_u, indicates that the acceleration should be minimized. The last term is a penalty on a slack variable for the safety.

The penalty coefficients, ϕ_s, ϕ_u, ϕ_v, and ϕ_ξ, are determined by the following logic. First, the penalty coefficient for the slack variable is determined as a relatively large value, $\phi_\xi = 100$, because the slack variable is introduced to address numerical feasibility issues from hard constraints; therefore, it is preferred to be minimized as much as is feasible due to safety concern. Then, the minimization of acceleration is scaled with that of the slack variable by considering the maximum magnitude of acceleration and the maximum of the slack variable: $\phi_u = \phi_{\xi_1} \cdot (d^*/u_{\max})^2$. Here, the marginal distance gap d^* is the desired maximum value of ξ. Similarly, the penalty coefficient on the desired speed tracking, ϕ_v, is determined: $\phi_v(t) = \phi_a \cdot (u_{\max}/v^*(t))^2$. ϕ_v is a time varying coefficient, since the speed limit changes on different road sections. Finally, the penalty coefficient on the desired headway tracking, ϕ_s, is selected as $\phi_a \cdot (u_{\max}/T_h^* v_{\max})^2$.

The target vehicle's acceleration is estimated as follows:

$$\hat{a}^{TV}(k-1|t) = \frac{1}{T_s}(\hat{v}^{TV}(k|t) - \hat{v}^{TV}(k-1|t)). \tag{10}$$

where $\hat{v}^{TV}$ is the future speed estimate of the target vehicle predicted by the ego vehicle. Then, the target vehicle position is integrated as follows during one-step integration:

$$\begin{aligned}
&\hat{s}^{TV}(k|t) \\
&= \hat{s}^{TV}(k-1|t) + T_s\hat{v}^{TV}(k-1|t) + 0.5T_s^2\hat{a}^{TV}(k-1|t) \\
&= \hat{s}^{TV}(k-1|t) + \frac{T_s}{2}\left[\hat{v}^{TV}(k-1|t) + \hat{v}^{TV}(k|t)\right]
\end{aligned}$$

The equality constraints (8f)-(8g) are derived from the vehicle dynamics with a point-mass system. More details on the MPC parameters are summarized in Tab. 2. The parameters are selected considering mid-size sedan vehicles. The marginal distance gap is determined to avoid collision, and the desired headway is determined considering safe time headway. The maximum and minimum acceleration and speed are determined considering vehicles' physical limitations.

5 Simulation Study

To evaluate the effect of the proposed weighting method in various driving environments, simulations are developed with real-world driving data as well as artificially-generated traffic by varying traffic conditions. This section provides detailed information including simulation set-up and baselines used for performance comparison and discussion of the results obtained in various driving situations.

5.1 Simulation Set-up

Only single-lane traffic is considered, and following vehicles behind the ego vehicle are not taken into account. Two types of traffic simulation are implemented:

1. Real-world traffic: Three vehicles' trajectories from the RWD-AA dataset are used.
2. Simulated traffic: Lead vehicles and the target vehicle drive the same standard drive cycles with deterministic time headway.

The real-world traffic from the RWD-AA data provides a realistic traffic condition, in which vehicles on the same lane drive with speed variations. Moreover, the performance of the eco-driving can be directly compared with human driving in a car-following scenario. On the other hand, the simulated traffic allows us to investigate the performance of the new prediction in various traffic environments by applying different drive cycles, different number of on-road vehicles, and different headway between vehicles. In this case, the V2V communication range is limited to 1 km. To consider various driving scenarios, five standard drive cycles are selected for analysis: the urban dynamometer driving schedule (UDDS), US06, the highway fuel economy test (HWFET), LA92, and the worldwide harmonized light vehicles test procedure (WLTP). Autonomie [30] is used to analyze the energy consumption in the powertrain of an electric vehicle. A midsize electric vehicle model with 300-mile range and fixed gear transmission is chosen for the analyses.

5.2 Prediction Horizon Length Selection

To determine the effective length of the prediction horizon, the eco-ACC is simulated with different prediction horizon lengths. Particularly, perfect previews on the target vehicle's speed over a prediction horizon are used in the eco-ACC. The eco-ACC performance is represented by the standard deviation of acceleration, since the objective function of the eco-ACC minimizes acceleration. In Fig. 11, the eco-ACC performances are presented with different prediction lengths. The results show that as the length of horizon increases, the standard deviation of acceleration decreases and converges at around 20 s for most drive cycles. This observation is in agreement with the finding in [2], in which eco car-following is realized by acceleration minimization. Electricity consumption (EC) is also reduced as the prediction horizon length increases, but converges faster than the acceleration. Based on these results, we select 20 s for the prediction horizon length as a conservative choice. The same value is also used for the control horizon length.

5.3 Baselines

For a quantitative analysis of the performance of the new predictor, constant speed and acceleration models are implemented as baseline strategies. Moreover, the polynomial regression without measurement weighting is implemented to test the efficacy of the new measurement weighting method. The prediction methods compared are summarized as follows:

1. Constant speed (CS), which uses the current speed of the target vehicle over the prediction horizon.
2. Constant acceleration (CA), which propagates the current acceleration of the target vehicle to generate a speed trajectory over the prediction horizon.
3. Polynomial regression with the least-square estimation (LS).
4. Polynomial regression with the weighted-least-square estimation (WLS).

Since the goal of the eco-ACC is to reduce energy consumption by automated driving, a human driver model is considered for performance comparison. The eco-ACC with the new predictor is compared with following trajectories of human drivers. For the real traffic simulation, the third vehicle of RWD-AA data is used as the baseline for the ego vehicle. For the simulated traffic, a baseline is generated by the intelligent driver model (IDM). IDM is a microscopic car-following model describing the crash-free responses of following drivers [24]. According to the IDM, the acceleration

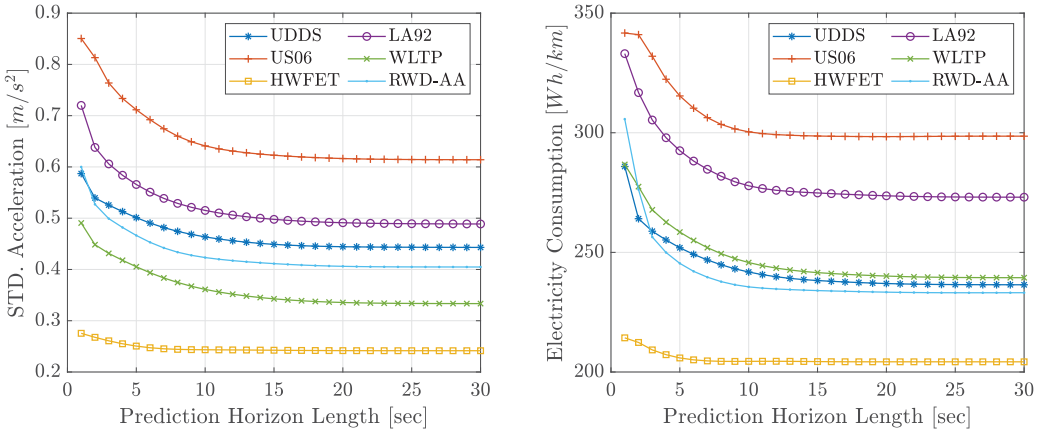

Fig. 11. Standard deviations of acceleration (left) and electricity consumption (right) with different prediction horizon lengths in the eco-ACC.

of the j^{th} vehicle can be modeled as follows:

$$\frac{dv_j}{dt} = \bar{a}\left[1 - \left(\frac{v_j(t)}{\bar{v}}\right)^{\delta} - \left(\frac{d^*(v_j, \Delta v_j)}{d_j(t)}\right)^2\right] \tag{11}$$

where v_j is the current longitudinal velocity of the j^{th} vehicle. $\bar{a}$ and $\bar{v}$ are the maximum acceleration and velocity, which should change according to different road characteristics. In this work, different values are chosen for these parameters for each standard drive cycle. The specific values of IDM parameters are presented in Tab. 3. Here, the parameter values are chosen to demonstrate general driving styles, i.e., not too aggressive or mild, by setting the maximum acceleration and speed to be similar to those of the original cycles.

In (11), d_j indicates the distance gap between the j^{th} vehicle and its preceding $(j-1)^{\text{th}}$ vehicle:

$$d_j(t) = s_{j-1}(t) - s_j(t) - L \tag{12}$$

where s_j is the one-dimensional location of the j^{th} vehicle and L is the length of a car, which is set to 4.5 m in our simulation. In (11), Δv_j is a relative speed between the j^{th} and the $(j-1)^{\text{th}}$ vehicle, such that:

$$\Delta v_j(t) = v_j(t) - v_{j-1}(t). \tag{13}$$

In (11), d^* is a desired distance gap between vehicles, defined as:

$$d^*(v, \Delta v) = d_0 + d_1\sqrt{\frac{v}{\bar{v}}} + T_h \cdot v + \frac{v\Delta v}{2\sqrt{\bar{a}\bar{b}}} \tag{14}$$

where d_0 and d_1 denote jam distances set to 2 m and zero, respectively, T_h represents a safe time headway chosen as 2 s, and $\bar{b}$ indicates the desired deceleration for passenger comfort, selected as 1.4 m/s^2. The acceleration exponent, δ, is set to 4 [33].

Table 3. IDM Parameter Values

	UDDS	US06	HWFET	LA92	WLTP
$\bar{a}$ [m/s^2]	1.5	3.8	1.5	3.1	1.8
$\bar{v}$ [m/s]	25	36	27	30	36

5.4 Simulation Results with the Real-World Traffic Data

The three vehicles' trajectories from the RWD-AA are used in this simulation. The first leading vehicle is a preceding vehicle as defined in Fig. 3, which shares its driving states to the ego vehicle through V2V communication. The second vehicle is considered the target vehicle. The third vehicle is used as a human baseline for the eco-ACC. The trajectories of the human-driven third vehicle and the eco-ACC driven one are compared in Fig. 12. In the subplots, the black lines represent the human baseline (the third vehicle's trajectories), and the red lines indicate the eco-ACC trajectories. The eco-ACC's velocity smoothing effect by acceleration minimization is shown in the speed and acceleration trajectories given in the first and second subplots from the top. The third and the fourth subplots from the top present the tracking performance by showing the distance gap and the time headway between the target vehicle and the ego vehicle. Since the eco-ACC formulation penalizes tracking performance in the cost function, the headway is within a reasonable range around the desired headway of 2 s. The simulations are terminated based on the predefined trip time. During the given time, the eco-ACC drives 7.9 m longer than the human driving. This demonstrates that the eco-ACC does not extend the trip time compared to the human driving.

The accuracy of the predictors is compared in Fig. 13. The left subplot provides the cumulative probability distributions of prediction errors over an entire prediction horizon, while the right subplot displays those at the first prediction step. Since the sampling time of our simulation is 1 s, these errors result from 1-s ahead predictions. Although

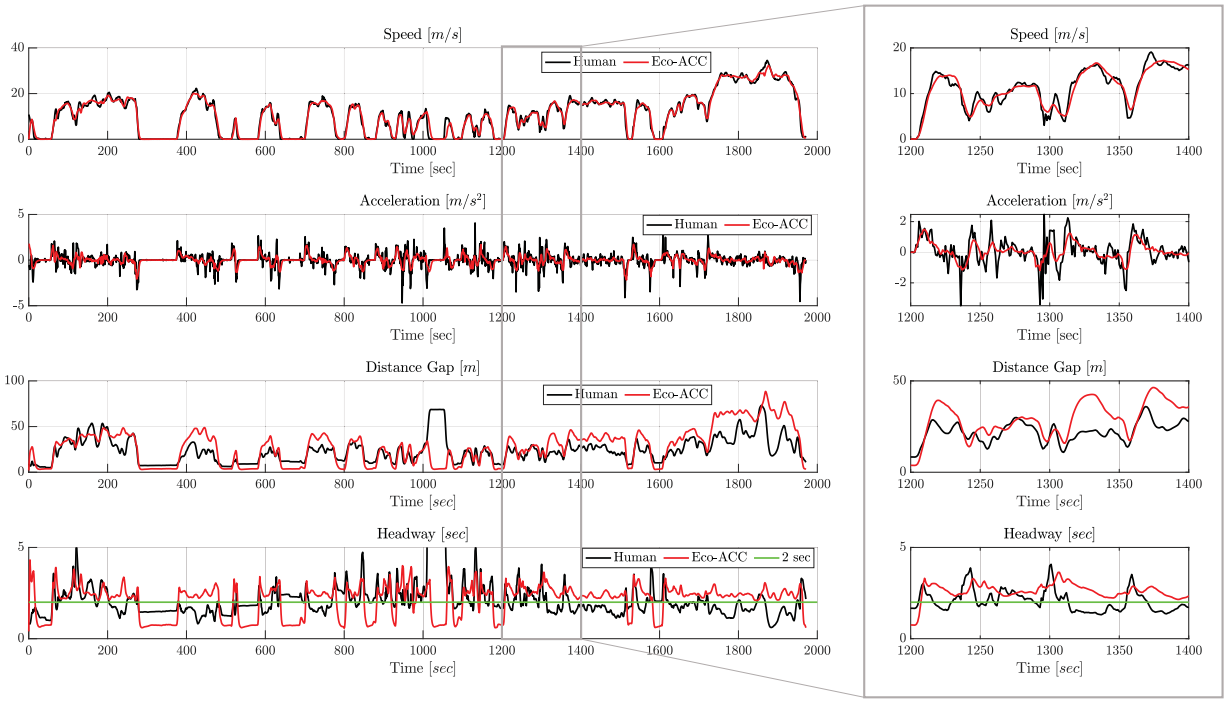

Fig. 12. Comparison between the trajectories driven by the real human driver in the Ann Arbor area (RWD-AA) and the simulated CAV using the eco-ACC given in Section 4.2 with the predictor based on WLS.

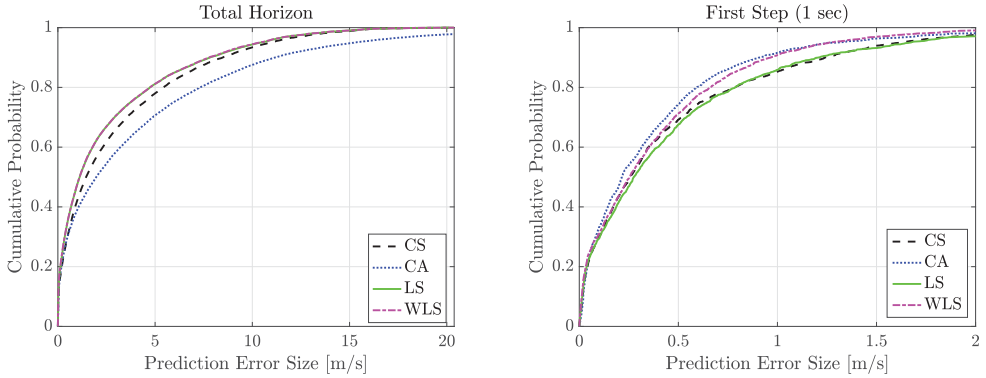

Fig. 13. Cumulative probability distributions of prediction errors from the entire prediction horizon (left) and the first prediction step (right).

WLS and LS seem to have almost the same accuracy for the entire prediction horizon, WLS outperforms LS at the first-step accuracy. This observation shows that the new measurement weighting improves the prediction accuracy at the near-future steps while not degrading overall accuracy, unlike CA does. CA has the highest accuracy for the first step, since CA propagates the most current acceleration sample, which is highly correlated with the acceleration a second later as shown in Fig. 7 and 8. However, this approach is not effective for addressing the rest of the horizon; CA results in the worst prediction performance compared to the other three methods.

In Fig. 14, the simulation results of the eco-ACC performed with different predictors are compared. In addition, the results from using perfect previews of the target vehicle's future speed are also compared as an ideal benchmark performance. These results are labeled as "Perfect" in the bar graphs. The left top subplot present the relative values of the standard deviation of longitudinal acceleration compared to the third human vehicle in RWD-AA data. Electricity consumption (EC) is compared in the right top subplot. The results show that the polynomial regression predictors outperform CS and CA in terms of acceleration minimization, and consequently electricity consumption saving.

The bottom subplots of Fig. 14 present tracking capability: mean time headway (left) and the mean magnitude of slack variables (right), ξ, imposed on the position constraint in (8b), respectively. By penalizing the 2-s headway tracking in the objective function (9), the time headway from the eco-ACC does not exceed 5 % variation from the human fol-

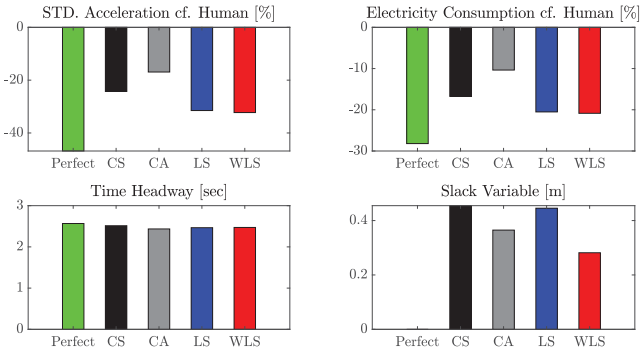

Fig. 14. Comparison of eco-ACC performance over the real traffic data (RWD-AA) with different prediction methods.

lowing with almost 30 % electricity consumption reduction. Here, the average time headway of the human following vehicle is 1.99 s. Thus, the eco-ACC follows the target vehicle with the reasonable range of distance gaps. The magnitude of the slack variables indicates the safety performance by showing the level of soft constraint violation. CA and WLS outperform the other two predictors because CA and WLS have high accuracy for the first-step prediction, which is the most critical for safety. However, the performance gaps between WLS and LS are not significant for the other aspects overall. Also, the electricity consumption saving by both polynomial regression predictors is 10% less compared to the benchmark performance ("Perfect"). This is due to the limited availability of measurements; the V2V messages from only one preceding vehicle are given in the RWD-AA data. Thus, to assess the performance more thoroughly, the new and the baseline predictors are evaluated under various simulated traffic conditions and the results are discussed in the next section.

5.5 Simulation Results under Various Simulated Traffic Conditions

To assess the accuracy of the predictors, root-mean-square errors (RMSE) at each prediction step are compared in Fig. 15. In the subplots, the black lines with crosses are the results of the constant speed prediction, and the gray lines with circles are from the constant acceleration method. To evaluate the predictor's performance in various traffic conditions, we vary the number of preceding vehicles from 1 to 10 and the time headway between the vehicles from 1 to 4 s. In Fig. 15, the shaded areas present the range of RMSE with various traffic parameters when the least-square and the weighted-least-square estimation are used. The lines with diamond markers are the medians of RMSE from the polynomial regression using the least-square estimation. The lines with triangles correspond to the median of RMSE from polynomial regression with weighted least-square estimation.

For all standard drive cycles, WLS has the highest accuracy up to 15 s, while sacrificing a little accuracy at the end of the horizon. LS also outperforms CS and CA, except for the first few prediction steps. The worst accuracy of the polynomial regression predictors are almost the same. The worst accuracy corresponds to the case when only one preceding vehicle's data is available and driving with 1-s time headway. In this case, most of the steps in a prediction horizon cannot be covered by V2V data points. According to our polynomial regression predictor's logic introduced in Section 2, the rest of the prediction horizon steps is addressed by propagating the current speed of the target vehicle. Consequently, the worst accuracy of LS and WLS are almost the same with the accuracy of CS.

The performance of the eco-ACC using different predictors is compared in Fig. 16. In the bar graphs, the green bars present simulation results using perfect previews on the target vehicle's speed over a prediction horizon, which is considered as the ideal benchmark performance. The clouds of black dots on the bars of LS (blue) and WLS (red) plot the eco-ACC performance with various traffic parameters: the number of preceding vehicles from 1 to 10, and the time headway between every preceding car from 1 to 4 s.

The top left subplot presents the standard deviation of acceleration compared to that of the IDM-driven trips. The results show that WLS achieves the largest improvement from the baseline except the perfect preview case. This improvement is reflected to electricity use as presented in the top right subplot. The simulation results show that WLS reduces electricity consumption the most among the predictors except the case using perfect previews, which is by up to 15% compared to the baseline.

One general concern for the eco-ACC is that it could sacrifice tracking performance. The bottom left subplot of Fig. 16 provides the tracking performance in terms of mean time headway compared to the IDM baseline. In the graph, the time headway of the eco-ACC ranges from 2.3 to 2.7 s. Considering the recommended time headway for safety is generally considered as 2 s, the eco-ACC in this work can maintain reasonable and safe time headway from the target vehicle.

The mean magnitudes of the slack variable, ξ, in the inequality constraint (8b) are compared in the bottom right subplot of Fig. 16. Overall, CA produces the smallest slack variables except the perfect preview case, because CA has the least RMSE at the first prediction step as shown in Fig. 15. Due to the same reason, WLS also results in small slack variables, especially compared to LS. Thus, WLS is the most effective prediction approach by minimizing electricity consumption most considerably among the other predictors while not significantly sacrificing tracking performance and maintaining the safety.

The electricity consumption from using LS and WLS is compared with various traffic conditions in Fig. 17. The results show that using WLS can achieve up to 4.7% more energy saving than LS. The largest improvement is mostly made when the entire horizon is fully covered by the V2V data, where the number of vehicles is larger and the time headway is longer. Hence, obtaining sufficient number of measurements would be crucial to maximize the advantage of the new prediction method.

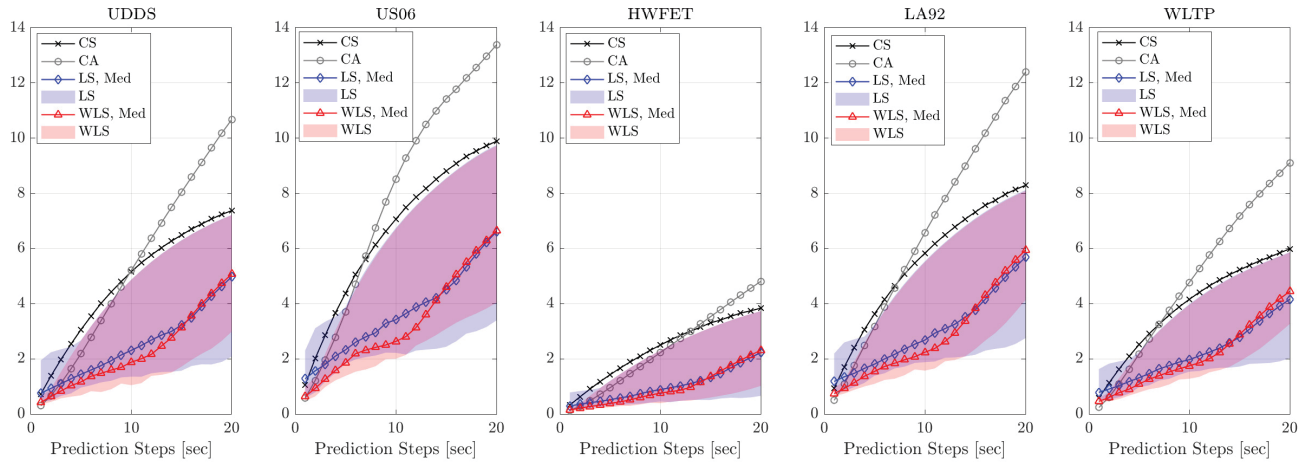

Fig. 15. Comparison of root-mean-square errors (RMSE) of prediction accuracy by prediction steps. The shaded areas are results from the variation in traffic simulation parameters: the number of preceding vehicles from 1 to 10, and the time headway from 1 to 4 s. The lines with the diamond and triangle markers indicate the medians of simulation results with traffic variations. In RWD-AA, the number of preceding vehicles was 1 and the average time headway was 2 s.

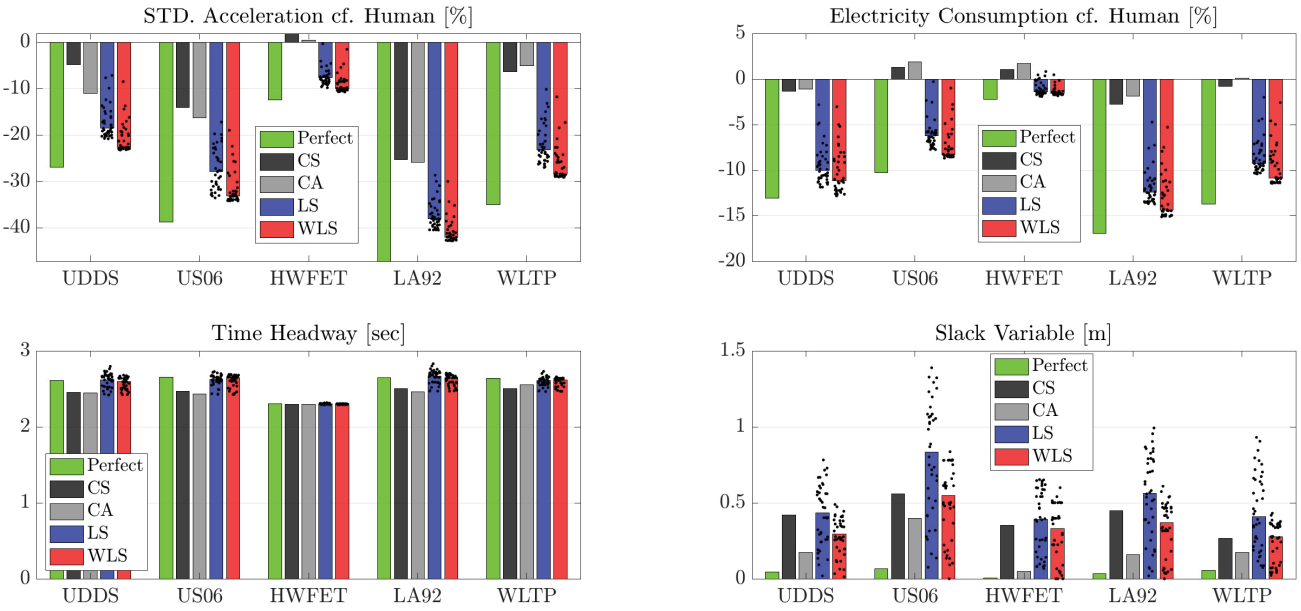

Fig. 16. Comparison of the eco-ACC performance with different speed prediction methods. The clouds of black dots show results from various traffic simulation parameters ($1 \leq N_{PV} \leq 5$ and $1 \leq T_h \leq 4$ s).

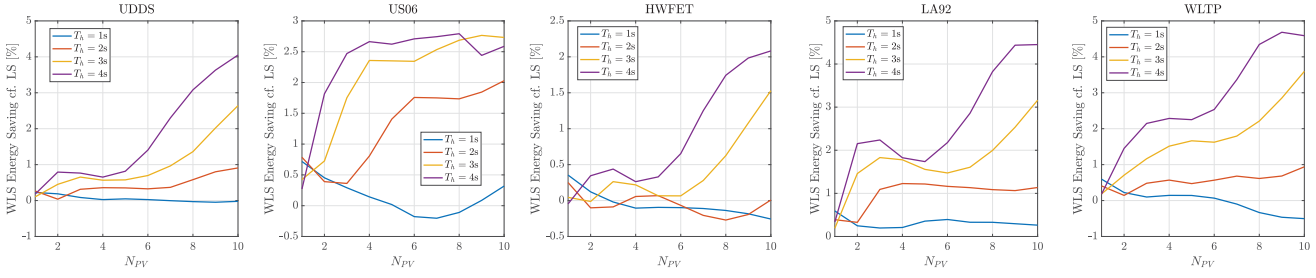

Fig. 17. Relative values of electricity consumption by using the weighted-least-square method compared to the least-square method.

6 CONCLUSIONS

This paper develops a novel measurement weighting strategy for vehicle speed forecasting to prioritize information obtained from different timing and sources. The temporal correlations in human driving states are investigated

by analyzing actual driving trajectories recorded from multiple drivers and DSRC basic safety messages. The forgetting factor and discount factor are defined to address the correlation trends and determine weights on the target vehicle's past speed and the preceding vehicle's current speed, respectively. Unlike machine-learning techniques that extract features from physical inputs, the proposed method is based on the intuitive characteristics of real-world driving, which can be easily modified for applications. The developed weighting method is applied to the vehicle speed predictor based on the polynomial regression, and validated in the real-world traffic scenario. Moreover, the performance reliability is validated by simulations in various driving environments. The efficacy of the predictor is tested by implementing the eco-ACC application in an MPC framework. The results reveal that the new predictor can reduce the energy consumption of an electric vehicle by up to 15% compared to human driving, and 10% compared to using constant speed/acceleration predictors. Furthermore, the developed weighting method improves energy consumption by 4.7% compared to using the polynomial regression without measurement weighting.

This paper studies an input layer design by proposing the measurement weighting strategy. Future work can extend the analyses by testing the proposed method with high measurement noise and loss of V2V packets. Investigation of the influence of CAV penetration on the performance and reliability of the method is also of interest. Finally, future efforts can focus on the output layer design of learning-based predictors by developing control-oriented loss functions.

ACKNOWLEDGMENTS

This work was partly funded by the Advanced Research Projects Agency-Energy (ARPA-E), U.S. Department of Energy, under Award Number DE-AR0000837. This material is based upon work supported by the National Science Foundation under Grant No. 1646019.

The authors would like to thank Toyota Motor North America Research & Development for providing the real-world driving data. The authors also would like to thank Professor Jim Sayer for sharing the real-world driving records collected as a part of the UMTRI IVBSS project [31]. Finally, the authors would like to thank Southwest Research Institute for valuable discussions on this development.

Appendix: Solution of Polynomial Regression for Vehicle Speed Forecasting

This section explains the solution of polynomial regression for vehicle speed forecasting used in this work. The well-known analytic solution of problem (3) is as follows:

$$\beta(t) = \left(X(t)^T W(t) X(t)\right)^{-1} X(t)^T W(t) \mathbf{v}(t). \quad (15)$$

where $\mathbf{v}(t)$ is a speed measurement vector used at time t given by:

$$\mathbf{v}(t) = [v^{TV}(t - N_{past}T_s), \cdots, v^{TV}(t - T_s), v^{TV}(t), \quad (16)$$

$$v^{<1>}(t), v^{<2>}(t), \cdots, v^{<N_{PV}>}(t)]^T. \quad (17)$$

In the measurement vector, $v^{<j>}$ is the speed of the j^{th} preceding vehicle. N_{past} is the number of past speed measurements of the target vehicle, and N_{PV} denotes the number of V2V messages that the ego vehicle received. The length of past speed is limited to 10 s adopted from [10]. The history for past measurements is reset when the target vehicle fully stops. The speed measurements of the target vehicle resume again once the target vehicle moves forward.

In (15), the design matrix $X(t)$ is composed of the polynomial basis of each measurement:

$$X(t) = \begin{bmatrix} 1 & N_{past}T_s & (N_{past}T_s)^2 \\ \vdots & \vdots & \vdots \\ 1 & 0 & 0 \\ \hline 1 & T_h^{<1>}(t) & T_h^{<1>}(t)^2 \\ \vdots & \vdots & \vdots \\ 1 & T_h^{<N_{PV}>}(t) & T_h^{<N_{PV}>}(t)^2 \end{bmatrix} \cdot \begin{matrix} \left.\vphantom{\begin{matrix}1\\\vdots\\1\end{matrix}}\right\}\text{Past} \\ \left.\vphantom{\begin{matrix}1\\\vdots\\1\end{matrix}}\right\}\text{Future} \end{matrix}$$

Note that the dimension of $X(t)$ may vary over time since the size of column vectors is determined by the number of data sampled every time.

References

[1] Wang, M., Daamen, W., Hoogendoorn, S. P., and van Arem, B., 2012. "Driver assistance systems modeling by model predictive control". In IEEE International Conference on Intelligent Transportation Systems, pp. 1543–1548.

[2] Prakash, N., Cimini, G., Stefanopoulou, A. G., and Brusstar, M. J., 2016. "Assessing fuel economy from automated driving: Influence of preview and velocity constraints". In ASME Dynamic Systems and Control Conference, pp. V002T19A001–V002T19A001.

[3] Sakhdari, B., Vajedi, M., and Azad, N. L., 2016. "Ecological adaptive cruise control of a plug-in hybrid electric vehicle for urban driving". In IEEE International Conference on Intelligent Transportation Systems, pp. 1739–1744.

[4] He, C. R., and Orosz, G., 2017. "Saving fuel using wireless vehicle-to-vehicle communication". In American Control Conference, pp. 4946–4951.

[5] Asher, Z. D., Baker, D. A., and Bradley, T. H., 2017. "Prediction error applied to hybrid electric vehicle optimal fuel economy". *IEEE Transactions on Control Systems Technology*(99), pp. 1–14.

[6] Hyeon, E., Kim, Y., Prakash, N., and Stefanopoulou, A. G., 2019. "Influence of speed forecasting on the performance of ecological adaptive cruise control". In ASME Dynamic Systems and Control Conference.

[7] Guo, J., He, H., and Sun, C., 2019. "ARIMA-based road gradient and vehicle velocity prediction for hybrid electric vehicle energy management". *IEEE Transactions on Vehicular Technology,* **68**(6), pp. 5309–5320.

[8] Liu, K., Asher, Z., Gong, X., Huang, M., and Kolmanovsky, I., 2019. Vehicle velocity prediction and energy management strategy part 1: Deterministic and stochastic vehicle velocity prediction using machine learning. Tech. rep., SAE Technical Paper.

[9] Hellström, E., and Jankovic, M., 2015. "A driver model for velocity tracking with look-ahead". In American Control Conference, pp. 3342–3347.

[10] Nüesch, S. P., Sterniak, J., Jiang, L., and Stefanopoulou, A. G., 2015. "On beneficial mode switch decisions based on short-term engine load prediction". *IFAC-PapersOnLine,* **48**(15), pp. 159–166.

[11] Lefèvre, S., Sun, C., Bajcsy, R., and Laugier, C., 2014. "Comparison of parametric and non-parametric approaches for vehicle speed prediction". In American Control Conference, pp. 3494–3499.

[12] Sun, C., Hu, X., Moura, S. J., and Sun, F., 2015. "Velocity predictors for predictive energy management in hybrid electric vehicles". *IEEE Transactions on Control Systems Technology,* **23**(3), pp. 1197–1204.

[13] Lemieux, J., and Ma, Y., 2015. "Vehicle speed prediction using deep learning". In IEEE Vehicle Power and Propulsion Conference, pp. 1–5.

[14] Zhang, F., Xi, J., and Langari, R., 2016. "Real-time energy management strategy based on velocity forecasts using V2V and V2I communications". *IEEE Transactions on Intelligent Transportation Systems,* **18**(2), pp. 416–430.

[15] Olabiyi, O., Martinson, E., Chintalapudi, V., and Guo, R., 2017. "Driver action prediction using deep (bidirectional) recurrent neural network". *arXiv preprint arXiv:1706.02257*.

[16] Di Cairano, S., Bernardini, D., Bemporad, A., and Kolmanovsky, I. V., 2014. "Stochastic MPC with learning for driver-predictive vehicle control and its application to HEV energy management". *IEEE Transactions on Control Systems Technology,* **22**(3), pp. 1018–1031.

[17] Zhang, C., and Vahidi, A., 2011. "Predictive cruise control with probabilistic constraints for eco driving". In ASME Dynamic Systems and Control Conference, Vol. 54761, pp. 233–238.

[18] Moser, D., Waschl, H., Schmied, R., Efendic, H., and del Re, L., 2015. "Short term prediction of a vehicle's velocity trajectory using ITS". *SAE International Journal of Passenger Cars-Electronic and Electrical Systems,* **8**(2015-01-0295), pp. 364–370.

[19] Oh, G., and Peng, H., 2019. "Impact of traffic lights on trajectory forecasting of human-driven vehicles near signalized intersections". *arXiv preprint arXiv:1906.00486*.

[20] Jing, J., Filev, D., Kurt, A., Özatay, E., Michelini, J., and Özgüner, Ü., 2017. "Vehicle speed prediction using a cooperative method of fuzzy Markov model and auto-regressive model". In IEEE Intelligent Vehicles Symposium, pp. 881–886.

[21] Jiang, B., and Fei, Y., 2016. "Vehicle speed prediction by two-level data driven models in vehicular networks". *IEEE Transactions on Intelligent Transportation Systems,* **18**(7), pp. 1793–1801.

[22] Vajedi, M., and Azad, N. L., 2016. "Ecological adaptive cruise controller for plug-in hybrid electric vehicles using nonlinear model predictive control". *IEEE Transactions on Intelligent Transportation Systems,* **17**(1), pp. 113–122.

[23] Kamal, M. A. S., Mukai, M., Murata, J., and Kawabe, T., 2013. "Model predictive control of vehicles on urban roads for improved fuel economy". *IEEE Transactions on Control Systems Technology,* **21**(3), pp. 831–841.

[24] Treiber, M., Hennecke, A., and Helbing, D., 2000. "Congested traffic states in empirical observations and microscopic simulations". *Physical Review E,* **62**(2), p. 1805.

[25] Gong, Q., Li, Y., and Peng, Z.-R., 2008. "Trip based near globally optimal power management of plug-in hybrid electric vehicles using gas-kinetic traffic flow model". *IFAC Proceedings Volumes,* **41**(2), pp. 4665–4670.

[26] Asadi, B., Zhang, C., and Vahidi, A., 2010. "The role of traffic flow preview for planning fuel optimal vehicle velocity". In ASME Dynamic Systems and Control Conference, Vol. 44182, pp. 813–819.

[27] Jing, J., Kurt, A., Ozatay, E., Michelini, J., Filev, D., and Ozguner, U., 2015. "Vehicle speed prediction in a convoy using V2V communication". In IEEE International Conference on Intelligent Transportation Systems, pp. 2861–2868.

[28] Hyeon, E., Kim, Y., Prakash, N., and Stefanopoulou, A. G., 2019. "Short-term speed forecasting using vehicle wireless communications". In American Control Conference, pp. 736–741.

[29] Hyeon, E., Shen, D., Karbowski, D., and Rousseau, A., 2021. Forecasting short to mid-length speed trajectories of preceding vehicle using V2X connectivity for eco-driving of electric vehicles. Tech. rep., SAE Technical Paper.

[30] Argonne National Laboratory. Autonomie. Accessed Aug. 24, 2021, http://www.autonomie.net/.

[31] Sayer, J., LeBlanc, D., Bogard, S., Funkhouser, D., Bao, S., Buonarosa, M. L., and Blankespoor, A., 2011. Integrated vehicle-based safety systems field operational test: Final program report. Tech. rep., United States. Joint Program Office for Intelligent Transportation Systems.

[32] The Insurance Institute for Highway Safety. Maximum posted speed limits by state. Accessed Aug. 24, 2021, https://www.iihs.org/topics/speed/speed-limit-laws.

[33] Treiber, M., and Kesting, A., 2013. "Car-following models based on driving strategies". In *Traffic flow dynamics*. Springer, pp. 181–204.

